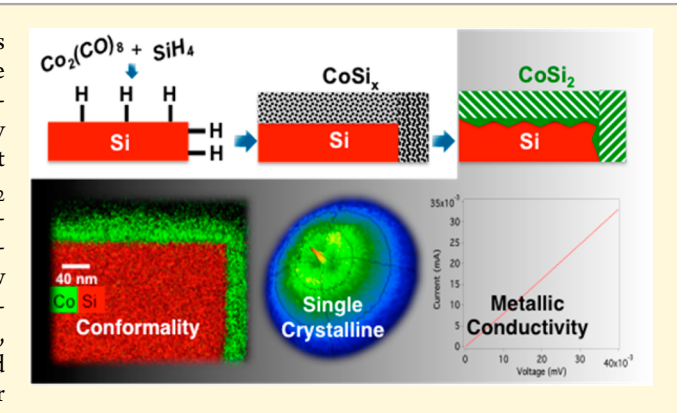


Conformal Deposition of Conductive Single-Crystalline Cobalt Silicide Layer on Si Wafer via a Molecular Approach

Tsung-Han Lin,[†] Tigran Margossian,[†] Li-Qing Zheng,[†] Sudhir Kumar,[†] Ivan Marozau,[⊥] Olha Sereda,[⊥] Dmitry Zemlyanov,^{||} Chih-Jen Shih,[†] Renato Zenobi,[†] David Baudouin,[†] Giovanni De Micheli,[‡] Pierre-Emmanuel Gaillardon,*,[§] and Christophe Copéret*,[†]

Supporting Information

ABSTRACT: The realization of metal-semiconductor contacts plays a significant role in ultrascaled integrated circuits. Here, we establish a low-temperature molecular approach for the conformal deposition of a 20 nm Co-rich layer on Si (100) wafers by reaction in solution of Co₂(CO)₈ with SiH₄. Postannealing at 850 °C under vacuum (~10⁻⁵ mbar) yields a crystalline CoSi₂ film with a lower surface roughness ($R_{\rm rms} = 5.3$ nm) by comparison with the conventional physical method; this layer exhibiting a metallic conductive behavior (ohmic behavior) with a low resistivity ($\rho = 11.6 \,\mu\Omega$ cm) according to four-point probe measurement. This approach is applicable to trench-structured wafers, showing the conformal layer deposition on 3D structures and showcasing the potential of this approach in modern transistor technology.



INTRODUCTION

The downscaling trend in microelectronics has led to the decrease of gate length in modern transistors down to values of 10 nm and below. 1-5 In parallel, 3D-transistor structures have been designed to optimize the electrostatic control and maximize the density of integration. 6-10 However, these advances point to the need of an alternative route in most of the fabrication steps to achieve an optimum performance in 3D-structured devices. This applies to metal silicides, which are needed to decrease the transistor contact resistivity. Of all metal silicides, cobalt silicide (CoSi₂) displays several advantages such as having a small lattice mismatch on Si substrate (\sim 1.2%), single crystallinity with epitaxial growth on Si, high thermal stability, and lower relative resistivity. 11,12 However, it is not widely used in industry because of the high-roughness issue ($R_{\rm rms}$ is always higher than 10 nm)¹³ resulting from large amounts of Si consumption during its formation with conventional physical methods, e.g., rapid thermal annealing after metal evaporation or sputtering. 11 Additionally, conventional physical methods result in limited conformality, i.e., limited homogeneity of the deposited layer throughout the targeted surface. As a result, atomic layer deposition (ALD) has been widely investigated because it yields a better conformality under a low-temperature process. 14-16 Nevertheless, the thermal instability of cobalt molecular precursors in gas-phase reactions is still a major challenge, which limits their applicability. 14 Recently, various electronic devices have been established on the basis of the synthesis of nanoparticles via colloidal approach. 17-19 Recent advances have shown that the metal silicides can be prepared at low temperatures²⁰ and that this approach can be used for the direct and conformal formation of nickel silicide via a low-temperature wet chemical approach.²¹ However, this nickel silicide displays ill-defined electrical properties due to the presence of resistive domains that cannot be removed upon

Here, we show that, by selecting an appropriate cobalt precursor, Co₂(CO)₈, and low-temperature in situ deposition conditions (SiH₄ at 55 °C in toluene with Si (100) wafer), a homogeneous and conformal cobalt silicide layer can be grown on Si substrates. After thermal annealing under vacuum, this layer contains a single-crystalline CoSi2 phase and displays the desired metallic conductive properties, showing an ohmic behavior with a low resistivity (11.7 $\mu\Omega$ cm; for comparison, the resistivity of bulk Co(0) metal equals 11.1 $\mu\Omega$ cm).²²

Received: February 15, 2018 Revised: February 21, 2018 Published: February 21, 2018



2168

Department of Chemistry and Applied Biosciences, ETH Zürich, Vladimir-Prelog-Weg 1-5, CH-8093 Zürich, Switzerland

^{*}Department of Electrical Engineering, EPF Lausanne, CH-1015 Lausanne, Switzerland

[§]Department of Electrical and Computer Engineering, University of Utah, Salt Lake City, Utah 84112, United States

Brick Nanotechnology Center, Purdue University, West Lafayette, Indiana 47907-2057, United States

^LCSEM SA, Jaquet-Droz 1, CH-2002 Neuchâtel, Switzerland

■ RESULTS AND DISCUSSION

The reaction of $Co_2(CO)_8$ (0.035 mmol) and SiH_4 (0.33 mmol) in toluene at 55 °C with Si (100) wafer (Figure 1a) leads to the

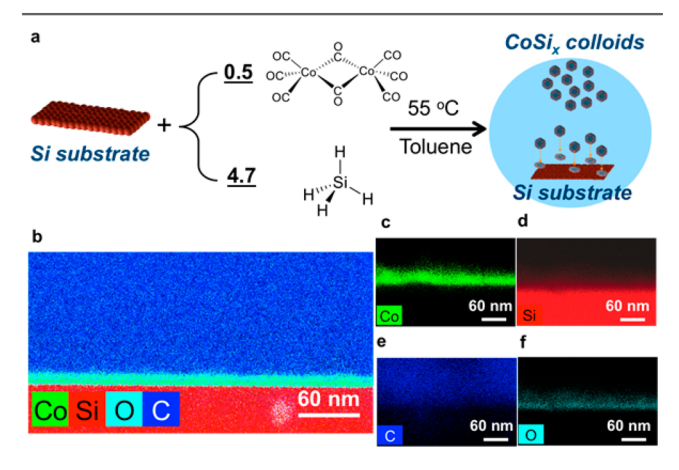


Figure 1. (a) Reaction scheme for one-pot synthesis; the condition is as below: $Co_2(CO)_8$ /die, $110\,000\,$ Co nm^{-2} , SiH_4 /Co = 4.7 with toluene at 55 °C for 16 h. (b) EDS mapping image of the Co-rich layer on the Si substrate. (c-f) Co, Si, C, and O EDS mapping images of the Co-rich layer on the Si substrate, respectively. The wafer was exposed to air prior to analysis.

homogeneous deposition of a ca. 20 nm Co-rich layer on the Si (100) wafer (Figure 1b) along with 3.5 nm colloids remaining in solution (Figure S1a,b). The transmission Fourier transform infrared spectroscopy (FTIR) analysis of the gas phase clearly shows the presence of unreacted SiH_4 (2180 cm⁻¹) and a large amount of CO (2140 cm⁻¹), ^{23,24} consistent with the reaction of Co₂(CO)₈ with presumably SiH₄ (Figure S1d). Quantification by gas chromatography-mass spectrometry (GC-MS) indicates the release of ca. 7.6 equiv of CO per Co₂(CO)₈. Energydispersive X-ray spectroscopy (EDS) mapping (Figure 1b) shows that the layer homogeneously contains Co (Figure 1c) and Si (Figure 1d) along with a small amount of carbon (Figure 1e) and oxygen (Figure 1f). The presence of oxygen likely results from the formation of CoSi, O, species upon exposure to air during the ex situ transfer (vide infra). Further analysis of the deposited layer by FTIR shows the presence of a peak at 2010 cm⁻¹ associated with the presence of remaining CO ligand bound to Co (Figure S1e).

X-ray photoelectron spectroscopy (XPS) depth profile (Figure 2a) confirms the homogeneous composition of the Co-rich layer, which is composed of similar amounts of Co and Si (average 20% and 23% in the first 20 nm, respectively), along with 8% carbon and 49% oxygen, consistent with EDS results discussed above. Within the depth of 20 nm (detailed XPS data of whole depth in Figure S2), Co 2p3 XPS spectra (Figure S2a) show a broad peak at around 778.2-778.4 eV, indicating the presence of different oxidized cobalt species in this layer. 25,26 The main Si 2p peak is at ~103 eV (Figure S2b), and the O 1s peak is at ~532.4 eV (Figure S2c), which is significantly different from SiO₂ (103.3 eV for Si 2p and 532.7 for O 1s), ^{27,28} indicating the formation of CoSi_xO_y species as discussed above (Figure 1f). From C 1s spectra (Figure S2d), a broad carbon signal appears at 284.0-286.0, including sp² carbon (284.5 eV) with some sp³ carbon or oxidized sp² carbon (285.4 eV).²⁹ This signal probably originates from the background of the pristine Si wafer, which also exhibits \sim 9% carbon with the similar peak position (Figure S3), or from the embedded CO ligand from Co precursor (Figure S1e).

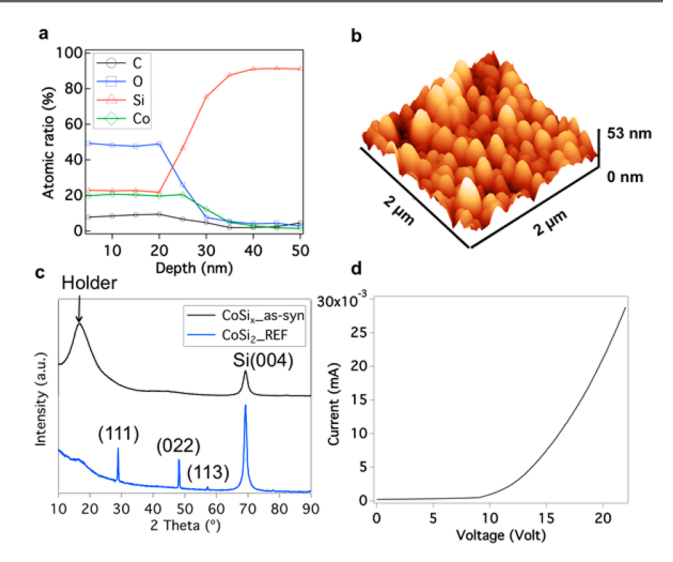


Figure 2. (a) XPS depth profile quantification on the as-synthesized wafer. (b) AFM image of as-synthesized CoSi_x layer on the Si substrate. (c) X-ray diffraction patterns of CoSi_x on $\operatorname{Si}(100)$ substrate: as-synthesized sample (black curve) and reference CoSi_2 by conventional method (blue curve) with Miller index shown for Si and CoSi_2 crystalline peaks. (d) I-V characteristics of as-synthesized CoSi_x layer on the Si(100) wafer.

These XPS data provide evidence of the homogeneous distribution of Co and Si in the layer. X-ray absorption spectroscopy (XAS) analysis was conducted on a model substrate with high surface area, e.g., Si(0) nanoparticles, in place of Si wafer to obtain spectroscopic data with better quality, which are consistent with the formation of CoSi_x. The observed edge shift at the Co K edge with respect to Co(0) foil indicates that this film is composed of $CoSi_r$ instead of Co(0), and the energy shift is attributed to the charge redistribution for the CoSi_r formation (Figure S4c). The atomic force microscopy (AFM) image reveals that the as-synthesized CoSi, layer is composed of large domains (Figure 2b), associated with the aggregation of CoSi, colloidal nanoparticles on the substrate, as made evident by the rootmean-square roughness (R_{rms}) of 8.5 nm. X-ray diffraction (XRD) on the as-synthesized layer does not show any crystalline domain, consistent with the formation of amorphous CoSi_x (Figure 2c). This CoSi, layer was then characterized by four-point probe measurement, and its current-voltage (I-V) behavior is shown in Figure 2d. The *I–V* curve exhibits Schottky characteristics, with a barrier height of 0.54 eV and series resistance of 147.1 Ω with an ideality factor of 115, obtained by using the thermionic emission model fitting (see the Supporting Information).³⁰ This ill-defined ideality factor, together with high sheet resistance, is the signature of an energy barrier formed because of voids or ligands between amorphous nanoparticles.

For removal of the residual carbon (such as CO ligands) and for the acquisition of a crystalline $CoSi_x$ layer, which should in turn provide the desired electrical properties, a thermal annealing is conducted under vacuum (for schematics, see Figure 3a) and monitored via XRD. While samples treated at various temperatures (350, 500, or 700 °C) under vacuum do not show crystalline $CoSi_x$ signals (Figure S5), raising the temperature to 850 °C (green curve in Figure 3b) leads to the appearance of two reflections at $2\theta = 34^\circ$ and 70° , associated with the $CoSi_2$ (002) and (004) planes, respectively, thus suggesting the formation of oriented single-crystalline $CoSi_2$ phase. This contrasts with the $CoSi_2$ obtained by the conventional method

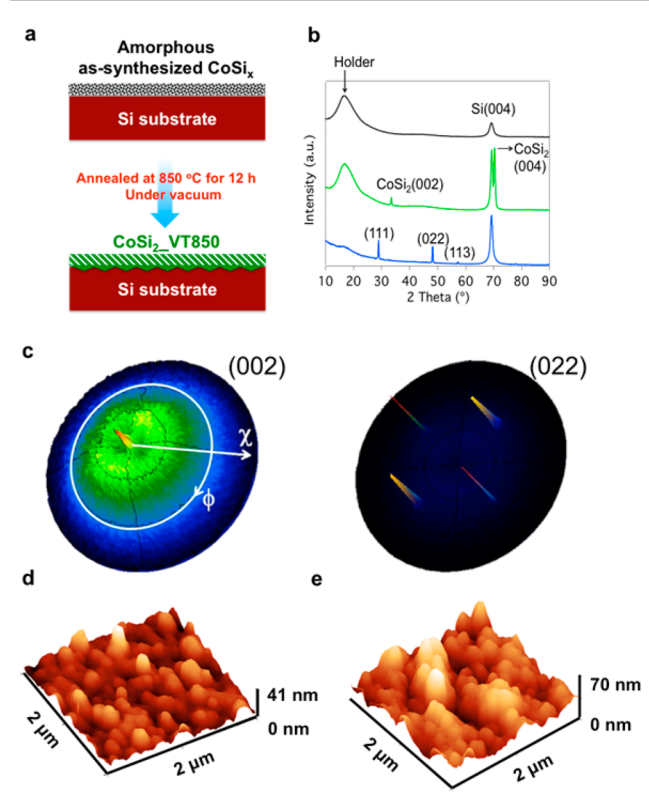


Figure 3. (a) Scheme of the annealing process in this work; the conditions are as below: as-synthesized sample was annealed at 850 °C for 12 h under vacuum. (b) X-ray diffraction patterns of $CoSi_x$ on Si(100) substrate: as-synthesized sample (black curve), samples after a 850 °C (green curve) thermal vacuum treatment, and reference $CoSi_2$ sample (blue curve) with Miller index shown for Si and $CoSi_2$ crystalline peaks. (c) Pole figures of (002) and (022) reflections of obtained $CoSi_2$ film. AFM images of $CoSi_x$ layer on the Si substrate: (d) sample after vacuum treatment at 850 °C, $R_{rms} = 5.3$ nm; (e) conventional $CoSi_2$ on wafer, $R_{rms} = 10.7$ nm.

(blue curve in Figure 3b, experimental details in the Supporting Information), which reveals three major reflections at $2\theta = 29^{\circ}$, 48°, and 57°, assigned to CoSi, (111), (022), and (113) planes, respectively, consistent with the formation of polycrystalline CoSi₂. For a further study of the epitaxial relationship of obtained CoSi₂ film on Si substrate after annealing at 850 °C under vacuum, pole figures were acquired for the CoSi₂ (002) and (022) diffraction reflections (Figure 3c). The (002) pole figure reveals only one peak in the out-of-plane direction (the tilted angle, $\chi = 0^{\circ}$; the rotation angle, $\varphi = 0^{\circ}$), proving a preferred {001} orientation in this direction. The (022) pole figure reveals four strong peaks at $\chi = 45^{\circ}$ and $\varphi = 45^{\circ}$, 135° , 225° , 315° . The observed tilt of 45° perfectly matches to the theoretical angle between (002) and (022) planes for a cubic unit cell. The appearance of four discrete peaks at φ increments of 90° indicates a high degree of in-plane orientation of the obtained CoSi₂ film, suggesting a nearly perfect cube-on-cube epitaxial relationship between the film and Si substrate. XRD results show that single-crystalline CoSi2 can be formed via this wet deposition method after annealing; the single {100} out-of-plane orientation is probably the result of the excellent epitaxial growth after direct CoSi_x formation on Si (100) substrate. The formation of CoSi₂ after vacuum treatment is further confirmed by XAS based on a Si(0) model (Figure S4c), which reveals the presence of ca. 99.2% CoSi₂ and 0.8% Co(0). EDS mapping (Figure S6) shows that, after the treatment, a homogeneous layer contained Co

(Figure S6c) and Si (Figure S6d) along with some contaminations as described before. It is noted that Co tends to diffuse into the Si substrate during the thermal treatment, ³¹ as shown in this case. AFM image of this layer reveals that $R_{\rm rms}$ drops to 5.3 nm (Figure 3d) after thermal annealing under vacuum, consistent with an improvement of the film homogeneity in comparison with the as-synthesized ${\rm CoSi}_x$ layer (Figure 2b). Further, this value is greatly improved by comparison with ${\rm CoSi}_2$ ($R_{\rm rms}$ = 10.7 nm, Figure 3e) prepared by the physical method, which is due to the interdiffusion of Co(0) metal and Si substrate during the typical rapid thermal annealing (RTA) process. ³²

The I-V characteristics are also significantly improved, compared to that in Figure 2d. Figure 4a presents an ohmic

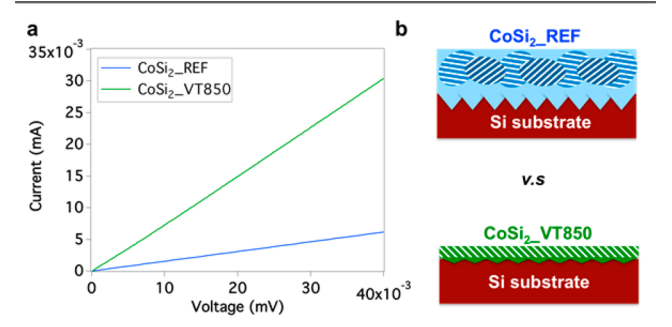


Figure 4. (a) I-V characteristics of the CoSi₂ layer deposited on a Si(100) wafer: green line, sample after 850 °C thermal vacuum treatment; blue line, reference CoSi₂ sample from conventional method. (b) Scheme of CoSi₂ from chemical method compared with CoSi₂ from conventional method.

I-V behavior with a low resistivity of $11.6~\mu\Omega$ cm (green line in Figure 4a). The I-V profile for the control $CoSi_2$ film prepared by the conventional physical method is also attached (blue line in Figure 4a), which only exhibits a resistivity of 55.6 $\mu\Omega$ cm. We infer that the low resistivity could be due to the formation of single-crystalline $CoSi_2$ (for schematics, see Figure 4b) upon thermal annealing, through healing the voids between amorphous nanoparticles, which directly benefit carrier transport.

Furthermore, this chemical method was utilized on trench-structured wafer to evaluate the conformality of this deposition method (reaction scheme shown as Figure 5a). The as-synthesized sample exhibited a conformal and homogeneous CoSi_x layer from EDS mapping, shown in Figures S8 and S9. Also, HAADF and EDS mapping of the trenched sample after post-treatment (Figure 5b–e) reveal the formation of the conformal CoSi₂ layer on the substrate (36–37 nm on all sides), illustrating that the post-treatment does not affect the homogeneous coverage of the 3D-structure Si substrate. HAADF and EDS mapping also show that Co diffuses into Si substrate to produce nanometric CoSi₂ pyramids within the interface between the CoSi₂ layer and the substrate (Figure 5c).

CONCLUSION

In summary, this work has allowed for the conformal deposition of an amorphous CoSi_x layer on a Si substrate via the reaction of $\mathrm{Co_2(CO)_8}$ and $\mathrm{SiH_4}$ in toluene at 55 °C. Postdeposition thermal annealing under vacuum generates the single-crystalline phase of $\mathrm{CoSi_2}$ with a {001}-preferred orientation onto the $\mathrm{Si(100)}$ substrate with a good surface roughness (R_{rms} = 5.3 nm), and displays metallic resistivity (11.6 $\mu\Omega$ cm; for bulk $\mathrm{Co(0)}$ metal, 11.1 $\mu\Omega$ cm). Therefore, this work establishes that molecular approaches are compatible with modern transistor

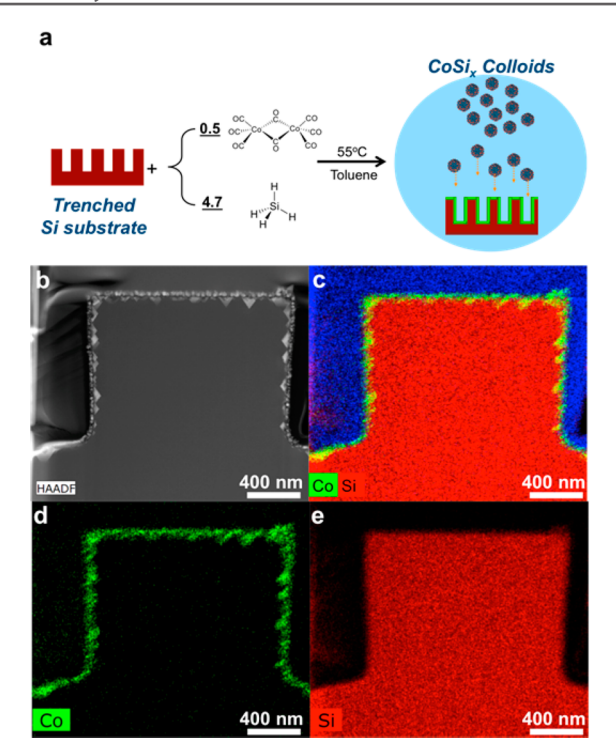


Figure 5. (a) Reaction scheme for one-pot synthesis on trench-structured wafer, and the conditions are as below: $\text{Co}_2(\text{CO})_8/\text{die}$, $110\,000\,\text{Co}\,\text{nm}^{-2}$, $\text{SiH}_4/\text{Co}=4.7$ with toluene at 55 °C for 16 h. (b) HAADF and (c) EDS mapping image of the CoSi_2 layer on the trenched Si substrate. (d, e) Co and Si EDS mapping images of the CoSi_2 layer on the Si substrate, respectively.

fabrication technologies, which could also be applied on 3D-structured devices with minimal sizes. We are currently exploring this possibility.

■ EXPERIMENTAL SECTION

General Information. The experiments were carried out using Schlenk techniques. Toluene was dried and collected using a mBraun SBS-800 purification system and degassed by Schlenk techniques (vacuum to 10^{-1} mbar and purged with dry Ar 10 times). A 40% HF solution was purchased from VWR. Si(0) nanopowder was purchased from US-nano with the size between 20 and 30 nm and with 98% purity. $\text{Co}_2(\text{CO})_8$ was purchased from Strem and used as received. The 1% SiH_4 (N5.0) in helium was purchased from PanGas. H₂ was purified over R3-11 BASF catalyst/MS 4 Å before use. Commercial CoSi_2 (99%) powder was purchased from Alfa Aesar and used as received.

Cobalt Silicide Colloidal Nanoparticle Synthesis on Si Wafer (One-Pot Synthesis). Double-sided polished p-type 4 in. Si wafers with (100) orientations were diced into $2 \text{ cm} \times 1 \text{ cm}$ dies, cleaned by a 40% HF solution for 60 s, and washed with deionized (DI) water to remove excess HF. The diced wafers were then dried under high vacuum ($\sim 10^{-5}$ mbar) at room temperature for 12 h.

A HF-treated diced Si-wafer and 12.4 mg of $\rm Co_2(CO)_8$ (0.04 mmol) were placed in a 325 mL Fischer–Porter bottle in a glovebox and dissolved in toluene (10 mL). The reactor was then pressurized under 2.7 bar of 1% $\rm SiH_4$ in He (0.33 mmol) and heated to 55 °C for 16 h, during which a layer was formed on top of the Si wafer accompanied by a dark solution (colloid formation). The colloidal solution was cannulated out of the reactor, and the Si wafer was washed 2 times with 10 mL of toluene. Prior to storage inside the glovebox, the as-synthesized wafer was dried under vacuum ($\sim 10^{-2}$ mbar) for 3 h.

Cobalt Silicide Layer via Co Evaporation Followed by the Rapid Thermal Annealing on Si Wafer (Conventional Method). Co metal layer was evaporated onto a HF-treated p-type 4 in. Si wafer with the (100) orientation. Rapid thermal annealing was then conducted at 800 °C for 20 min under H_2/N_2 atmosphere, from which the $CoSi_2$

layer formed between the interface of Co and Si. The remaining Co metal layer was removed by washing in a piranha solution.

Cobalt Silicide Colloidal Nanoparticle Synthesis on Si(0) Nanopowder (One-Pot Synthesis). First, 2.0 g of Si(0) nanopowder was reduced under a flow of pure hydrogen (100 mL min⁻¹) at 900 °C (1 °C min⁻¹) for 12 h to obtain a pristine Si–H surface (Figure S4b). Then, 50 mg of Si(0) nanopowder and 46.5 mg of Co₂(CO)₈ (0.14 mmol) were placed in a 325 mL Fischer–Porter reactor in a glovebox and dissolved in toluene (10 mL). The reactor was then pressurized under 2.7 bar of 1% SiH₄ in He (0.45 mmol) and heated to 55 °C for 16 h, during which the solution color turned to black. Inside a glovebox, the Si powder was separated from the solution using a filter and consecutively washed 3 times with 10 mL of toluene. The Si powder was dried under high vacuum (~10⁻⁵ mbar) for 3 h.

Vacuum-Treatment Condition. As-synthesized wafer or nanopowder was treated under high vacuum (10⁻⁵ mbar) at different temperatures (350, 500, 700, or 850 °C; 1 °C min⁻¹) for 12 h.

Characterization Techniques. *Transmission Electron Microscopy (TEM).* TEM images were taken with an FEI Tecnai Orisis ultrahigh vacuum transmission electron microscope. An energy-dispersive (EDS) detector was attached onto the FEI Tecnai Orisis instrument for elemental mapping analysis.

TEM Sample Preparation by a Tripod Method. The as-synthesized wafer was cleaved into two pieces of 2.5 × 1.8 mm, which were glued face-to-face using a Gatan G2 epoxy glue. The specimen was then mounted on the side of a tripod polisher, which was heated at 100 °C. For removal of most of the Si-bulk wafer, the polishing procedure was conducted using a series of plastic diamond lapping films, with grains of decreasing sizes (30, 15, 6, 1, 0.5, and 0.1 μ m), and a final step was polished on a felt-covered disc using the slurry of silica with 25 nm grain size. The specimen was then mounted on the bottom of a tripod polisher, which was heated at 100 °C. The glass support was perfectly flat-polished to ensure a correct 0.6° angle of the wedge-shaped specimen. The same polishing procedure was used for the bottom part leading to the appearance of interference fringes (electron transparency), and then, the specimen was glued on a Mo grid. After 12 h of drying, the grid was detached from the tripod using acetone to dissolve the glue, and the specimen was cleaned by acetone.

TEM Sample Preparation by Focused-Ion-Beam (FIB) Method. A TEM lamella was prepared by the in situ lift-out technique on a Zeiss NVision 40 FIB—SEM instrument. The lamella was thinned using 30 kV Ga+. For the 5 kV showering to reduce the thickness of the damage layer the lamella was tilted 10° into the beam.

Atomic Force Microscopy. The AFM measurements were conducted on a commercial AFM system (BioScope Catalyst, Bruker Nano, Santa Barbara, California) that is mounted onto an inverted confocal laser-scanning microscope (FluoView FV500, Olympus, Center Valley, Pennsylvania). The images shown in this study were obtained using tapping mode AFM with CT300R-25 cantilever probes (Nanoscience). The AFM images are 2 μ m² in size, with a resolution of 512 × 512 pixels, and a scan rate of 0.2 Hz.

Fourier Transformed Infrared Spectroscopy (FTIR). FTIR spectra of wafers were recorded in transmission mode on a Thermo Scientific, Nicolet 6700, instrument in which the measurements were performed under inert condition with a deuterated triglycine sulfate (DTGS) detector with 1000 averaged scans to achieve an optimal signal-to-noise ratio. FTIR spectra of nanopowders were recorded in transmission mode on a Bruker ALPHA-T FTIR spectrophotometer under inert condition.

X-ray Photon Spectroscopy (XPS). XPS depth profiles were recorded using a Kratos Axis Ultra DLD spectrometer with monochromic Al K α radiation (1486.6 eV). A commercial Kratos charge neutralizer was used to avoid nonhomogeneous electric charge and to achieve better resolution. The resolution measured as full width at half-maximum of the curve fitted photoemission peaks was approximately 1 eV. Binding energy (BE) values refer to the Fermi edge, and the energy scale was calibrated using Au $4f_{7/2}$ at 84.0 eV and Cu $2p_{3/2}$ at 932.67 eV. Samples were attached to a stainless-steel sample holder bar using a double-sided sticking Cu tape. XPS data were analyzed with CasaXPS software version 2313 Dev64. The C–C component of the C 1s peak was set to a binding energy of 284.8 eV to correct for the charging effect on each

sample. The atomic concentrations of the elements in the near-surface region were estimated taking into account the corresponding Scofield atomic sensitivity factors and inelastic mean free path (IMFP) of photoelectrons using standard procedures in the CasaXPS software. Depth profiling was conducted by step-by-step sputtering of a sample with a Kratos polyatomic sputtering gun operating in Ar mode at 5 keV, $I_{\rm ion} \approx 1~\mu$ A. Thickness of the layers was calibrated using the TEM measured thickness.

X-ray Absorption Spectroscopy (XAS). XAS data were collected at the X10DA (Super XAS) beamline at the Swiss Light Source, Villigen, Switzerland. Spectra were collected on pressed pellets optimized to 1 absorption length at the Co K-edge in transmission mode. The beamline energy axis was calibrated with a Co reference foil, in which energies are measured at the inflection point(s) of the absorption signal, and the precision on the energy of the edge is ± 0.5 eV in the 7659–7759 eV area. The spectra were background-corrected using the Athena software package.

X-ray Diffraction Spectroscopy (XRD). Samples were investigated by X-ray diffraction (XRD) using a PANalytical X'Pert Pro MRD diffractometer equipped with a parallel beam mirror and a point detector. XRD measurements in the $\theta/2\theta$ geometry were performed for the phase analysis of the samples and to evaluate the out-of-plane preferential orientation. An incident angle offset of -0.2° was applied to reduce the contribution of the very strong Si(004) substrate reflection. Pole figure XRD measurements were carried out to study in detail the preferred crystallographic orientation of the samples. The pole figure measurements were performed for the CoSi₂ (002) and (022) reflections at 2θ angles of \sim 33.5° and \sim 48.0°, respectively.

Electrical Performance Evaluation. For four-point probe measurement, four 100 nm gold (Au) electrodes were deposited to a circle-shaped layer (0.25 mm in radius; separate with each one by 1 mm) with a deposition rate of 5 ± 2 Å s⁻¹ by thermal evaporation of Au ingots under high vacuum ($\sim 10^{-5}$ mbar). The Au ingots (99.999%) were supplied by Kurt J. Lesker. A MBraun glovebox-integrated MBraun vacuum thermal evaporator was used for the Au evaporation. The probe station used for I-V characteristic measurement is a Signatone S1160 station, and the I-V data were acquired by a Keysight B1500 instrument with B1510A high-power source/monitor unit (HPSMU).

ASSOCIATED CONTENT

S Supporting Information

The Supporting Information is available free of charge on the ACS Publications website at DOI: 10.1021/acs.chemmater.8b00701.

Experimental details, *I–V* characteristics, XPS, XAS, XRD, and TEM-EDS mappings (PDF)

AUTHOR INFORMATION

Corresponding Authors

*E-mail: pierre-emmanuel.gaillardon@utah.edu.

*E-mail: ccoperet@ethz.ch.

ORCID

Sudhir Kumar: 0000-0002-2994-7084 Chih-Jen Shih: 0000-0002-5258-3485 Christophe Copéret: 0000-0001-9660-3890

Notes

The authors declare no competing financial interest.

ACKNOWLEDGMENTS

The authors are thankful for the financial support of Swiss National Science Foundation, Grant CR22I2_152955 and of the US National Science Foundation Grant 1644592. Maxime Thanmasack is thanked for primary TEM data. Scope M (Frank Krumeich and Joakim Reuteler) is acknowledged for TEM sample preparation and measurement. Ka Wing Chan is also thanked for acquiring the CoSi₂ XAS data.

REFERENCES

- (1) Ilatikhameneh, H.; Ameen, T.; Novakovic, B.; Tan, Y.; Klimeck, G.; Rahman, R. Saving Moore's Law Down To 1 nm Channels With Anisotropic Effective Mass. *Sci. Rep.* **2016**, *6* (1), 31501.
- (2) Franklin, A. D.; Luisier, M.; Han, S.-J.; Tulevski, G.; Breslin, C. M.; Gignac, L.; Lundstrom, M. S.; Haensch, W. Sub-10 nm Carbon Nanotube Transistor. *Nano Lett.* **2012**, *12*, 758–762.
- (3) Service, R. F. Is Silicon's Reign Nearing Its End? *Science* **2009**, 323, 1000–1002.
- (4) Yang, Y.; Ding, L.; Han, J.; Zhang, Z.; Peng, L.-M. High-Performance Complementary Transistors and Medium-Scale Integrated Circuits Based on Carbon Nanotube Thin Films. *ACS Nano* **2017**, *11*, 4124–4132.
- (5) Iwai, H. Roadmap for 22 nm and beyond. *Microelectron. Eng.* **2009**, *86*, 1520–1528.
- (6) Singh, N.; Agarwal, A.; Bera, L. K.; Liow, T. Y.; Yang, R.; Rustagi, S. C.; Tung, C. H.; Kumar, R.; Lo, G. Q.; Balasubramanian, N.; Kwong, D. L. High-performance fully depleted silicon nanowire (diameter /spl les/ 5 nm) gate-all-around CMOS devices. *IEEE Electron Device Lett.* **2006**, 27, 383–386.
- (7) Xu, J.; Oksenberg, E.; Popovitz-Biro, R.; Rechav, K.; Joselevich, E. Bottom-Up Tri-gate Transistors and Submicrosecond Photodetectors from Guided CdS Nanowalls. *J. Am. Chem. Soc.* **2017**, *139*, 15958–15967.
- (8) Tomioka, K.; Yoshimura, M.; Fukui, T. A III–V nanowire channel on silicon for high-performance vertical transistors. *Nature* **2012**, 488, 189–192.
- (9) Cress, C. D.; Datta, S. Nanoscale Transistors—Just Around the Gate? Science 2013, 341, 140–141.
- (10) Ferain, I.; Colinge, C. A.; Colinge, J.-P. Multigate transistors as the future of classical metal—oxide—semiconductor field-effect transistors. *Nature* **2011**, *479*, 310–316.
- (11) Chen, J.; Colinge, J. P.; Flandre, D.; Gillon, R.; Raskin, J. P.; Vanhoenacker, D. Comparison of TiSi₂,CoSi₂, and NiSi for Thin-Film Silicon-on-Insulator Applications. *J. Electrochem. Soc.* **1997**, *144*, 2437–2442.
- (12) Chiu, S.-P.; Yeh, S.-S.; Chiou, C.-J.; Chou, Y.-C.; Lin, J.-J.; Tsuei, C.-C. Ultralow 1/f Noise in a Heterostructure of Superconducting Epitaxial Cobalt Disilicide Thin Film on Silicon. *ACS Nano* **2017**, *11*, 516–525.
- (13) Zimmermann, S.; Zhao, Q. T.; Höhnemann, H.; Wiemer, M.; Kaufmann, C.; Mantl, S.; Dudek, V.; Gessner, T. Roughness improvement of the CoSi₂/Si-interface for an application as buried silicide. *Microelectron. Eng.* **2007**, *84*, 2537–2541.
- (14) Zaera, F. The Surface Chemistry of Atomic Layer Depositions of Solid Thin Films. *J. Phys. Chem. Lett.* **2012**, *3*, 1301–1309.
- (15) George, S. M. Atomic Layer Deposition: An Overview. *Chem. Rev.* **2010**, *110*, 111–131.
- (16) Zaera, F. The surface chemistry of thin film atomic layer deposition (ALD) processes for electronic device manufacturing. *J. Mater. Chem.* **2008**, *18*, 3521–3526.
- (17) Kagan, C. R.; Lifshitz, E.; Sargent, E. H.; Talapin, D. V. Building devices from colloidal quantum dots. *Science* **2016**, 353 (885), aac5523-1–aac5523-9.
- (18) Talapin, D. V.; Lee, J.-S.; Kovalenko, M. V.; Shevchenko, E. V. Prospects of Colloidal Nanocrystals for Electronic and Optoelectronic Applications. *Chem. Rev.* **2010**, *110*, 389–458.
- (19) Murray, C. B.; Kagan, C. R.; Bawendi, M. G. Synthesis and Characterization of Monodisperse Nanocrystals and Close-Packed Nanocrystal Assemblies. *Annu. Rev. Mater. Sci.* **2000**, *30*, 545–610.
- (20) Baudouin, D.; Szeto, K. C.; Laurent, P.; De Mallmann, A.; Fenet, B.; Veyre, L.; Rodemerck, U.; Copéret, C.; Thieuleux, C. Nickel—Silicide Colloid Prepared under Mild Conditions as a Versatile Ni Precursor for More Efficient CO₂ Reforming of CH₄ Catalysts. *J. Am. Chem. Soc.* **2012**, *134*, 20624–20627.
- (21) Lin, T.-H.; Margossian, T.; De Marchi, M.; Thammasack, M.; Zemlyanov, D.; Kumar, S.; Jagielski, J.; Zheng, L.-Q.; Shih, C.-J.; Zenobi, R.; De Micheli, G.; Baudouin, D.; Gaillardon, P.-E.; Copéret, C. Low-Temperature Wet Conformal Nickel Silicide Deposition for

Transistor Technology through an Organometallic Approach. ACS Appl. Mater. Interfaces 2017, 9, 4948–4955.

- (22) De Vries, J. W. C. Temperature and thickness dependence of the resistivity of thin polycrystalline aluminium, cobalt, nickel, palladium, silver and gold films. *Thin Solid Films* **1988**, *167*, 25–32.
- (23) Kolomiitsova, T. D.; Savvateev, K. F.; Shchepkin, D. N.; Tokhadze, I. K.; Tokhadze, K. G. Infrared Spectra and Structures of SiH4 and GeH4 Dimers in Low-Temperature Nitrogen Matrixes. *J. Phys. Chem. A* **2015**, *119*, 2553–2561.
- (24) London, J. W.; Bell, A. T. Infrared spectra of carbon monoxide, carbon dioxide, nitric oxide, nitrogen dioxide, nitrous oxide, and nitrogen adsorbed on copper oxide. *J. Catal.* **1973**, *31*, *32*–40.
- (25) Bernal-Ramos, K.; Saly, M. J.; Kanjolia, R. K.; Chabal, Y. J. Atomic Layer Deposition of Cobalt Silicide Thin Films Studied by in Situ Infrared Spectroscopy. *Chem. Mater.* **2015**, *27*, 4943–4949.
- (26) Sciortino, L.; Giannici, F.; Martorana, A.; Ruggirello, A. M.; Liveri, V. T.; Portale, G.; Casaletto, M. P.; Longo, A. Structural Characterization of Surfactant-Coated Bimetallic Cobalt/Nickel Nanoclusters by XPS, EXAFS, WAXS, and SAXS. *J. Phys. Chem. C* **2011**, *115*, 6360–6366.
- (27) Ono, L. K.; Behafarid, F.; Cuenya, B. R. Nano-Gold Diggers: Au-Assisted SiO₂-Decomposition and Desorption in Supported Nanocatalysts. *ACS Nano* **2013**, *7*, 10327–10334.
- (28) Reddy, B. M.; Khan, A.; Yamada, Y.; Kobayashi, T.; Loridant, S.; Volta, J.-C. Surface Characterization of CeO₂/SiO₂ and V₂O₅/CeO₂/SiO₂ Catalysts by Raman, XPS, and Other Techniques. *J. Phys. Chem. B* **2002**, *106*, 10964–10972.
- (29) Vander Wal, R.; Bryg, V. M.; Hays, M. D. XPS Analysis of Combustion Aerosols for Chemical Composition, Surface Chemistry, and Carbon Chemical State. *Anal. Chem.* **2011**, *83*, 1924–1930.
- (30) Lee, H.; Keun Lee, Y.; Nghia Van, T.; Young Park, J. Nanoscale Schottky behavior of Au islands on TiO₂ probed with conductive atomic force microscopy. *Appl. Phys. Lett.* **2013**, *103* (17), 173103.
- (31) Wang, H.; Zhang, Z.; Wong, L. M.; Wang, S.; Wei, Z.; Li, G. P.; Xing, G.; Guo, D.; Wang, D.; Wu, T. Shape-Controlled Fabrication of Micro/Nanoscale Triangle, Square, Wire-like, and Hexagon Pits on Silicon Substrates Induced by Anisotropic Diffusion and Silicide Sublimation. ACS Nano 2010, 4, 2901–2909.
- (32) Diale, M.; Challens, C.; Zingu, E. C. Cobalt self-diffusion during cobalt silicide growth. *Appl. Phys. Lett.* **1993**, *62*, 943–945.